Biomaterials 156 (2018) 238–247

Contents lists available at ScienceDirect

Biomaterials

journal homepage: www.elsevier.com/locate/biomaterials

Microenvironments to study migration and somal translocation in cortical neurons

Shifang Zhao [a, b, c], Wenqiang Fan [d, e], Xiang Guo [a], Longjian Xue [c], Benedikt Berninger [d, e], Marcelo J. Salierno [c, d, e, **], Aránzazu del Campo [a, b, c, *]

[a] INM - Leibniz Institute for New Materials, Campus D2 2, 66123 Saarbrücken, Germany
[b] Chemistry Department, Saarland University, 66123 Saarbrücken, Germany
[c] Max-Planck-Institute für Polymerforschung, Ackermannweg 10, 55128 Mainz, Germany
[d] Institute of Physiological Chemistry, University Medical Center of the Johannes Gutenberg University Mainz, Hanns-Dieter-Hüsch-Weg 19, 55128 Mainz, Germany
[e] Focus Program Translational Neuroscience, Johannes Gutenberg University Mainz, Langenbeckstrasse 1, 55131 Mainz, Germany

ARTICLE INFO

Article history:
Received 27 August 2017
Received in revised form
24 November 2017
Accepted 27 November 2017
Available online 28 November 2017

Keywords:
Somal translocation
Cerebral cortex
Cortical neurons
Neuronal migration
Corticogenesis

ABSTRACT

Migrating post-mitotic neurons of the developing cerebral cortex undergo terminal somal translocation (ST) when they reach their final destination in the cortical plate. This process is crucial for proper cortical layering and its perturbation can lead to brain dysfunction. Here we present a reductionist biomaterials platform that faithfully supports and controls the distinct phases of terminal ST *in vitro*. We developed microenvironments with different adhesive molecules to support neuronal attachment, neurite extension, and migration in distinct manners. Efficient ST occurred when the leading process of migratory neurons crossed from low-to high-adhesive areas on a substrate, promoting spreading of the leading growth cone. Our results indicate that elementary adhesive cell-substrate interactions strongly influence migratory behavior and the final positioning of neurons during their developmental journey. This *in vitro* model allows advanced experimentation to reveal the microenvironmental requirements underlying cortical layer development and disorders.

During the mammalian corticogenesis, neurons migrate long distances from their birthplace to their final destination [1–3]. New post-mitotic neurons at the ventricular (VZ) and subventricular zones (SVZ) first migrate along radial glial fibers in a mode frequently referred to as "locomotion" [4–6]. When the leading process of the migrating neuron reaches the cortical plate (CP), cells undergo terminal somal translocation (ST). Cells detach from the radial fibers and complete their migration beneath the marginal zone (MZ) [5,7]. Terminal ST is believed to be used by late-generated neurons to make a final adjustment of their destination and adopted by early-generated neurons to migrate directly to their final position [8,9]. This process shows characteristic features: Initially, neurons develop a prominent leading process with a growth cone (GC) structure that explores the properties of the surrounding microenvironment. When the GC reaches the final destination, it spreads and anchors within the CP. Finally, the nucleus and surrounding organelles translocate towards the tip of the leading process [5,7,9].

Despite extensive studies on the topic, the guidance cues that trigger growth GC spreading and terminal ST that determines the final destination of migrating neurons remain unclear. The expression of particular extracellular molecules was found to play a critical role in directing neuronal migration [8,10–13]. The most studied one is Reelin, a key regulator in mammalian cortical lamination [14–19] and terminal ST [9,20,21]. The interplay between Reelin and the adhesion receptors integrin α5β1, α3β1 and N-cadherin has been documented [15,22–25]. Control of cellular migration processes through the regulation of membrane adhesive receptors seems logical [1]. Binding of cell adhesive receptors to extracellular counterparts is fundamental to cellular locomotion, and the spatial distribution of adhesive ligands in the extracellular matrix and/or on neighboring cells

* Corresponding author. INM - Leibniz Institute for New Materials, Campus D2 2, 66123 Saarbrücken, Germany.
** Corresponding author. Institute of Physiological Chemistry, University Medical Center of the Johannes Gutenberg University Mainz, Hanns-Dieter-Hüsch-Weg 19, 55128 Mainz, Germany.
E-mail addresses: salierno@gmail.com (M.J. Salierno), aranzazu.delcampo@leibniz-inm.de (A. del Campo).

https://doi.org/10.1016/j.biomaterials.2017.11.042
0142-9612/

can guide migration direction and persistence [26–29]. In this context, spatial localization of extracellular adhesive cues could be an effective regulator of neuronal positioning during corticogenesis.

Reports on neuronal migration *in vitro* are mostly based on spontaneously occurring neuronal locomotion in cell cultures, with no control on the migration mode [30,31]. Although recent studies have highlighted the sensitivity of neuronal migration to the properties of the underlying substrate [32,33], the concrete factors that control, trigger or direct ST to re-locate neuronal cells at pre-designated positions *in vivo* or *in vitro* remain unknown. Interesting experimental observations in an older report demonstrated that neuronal migration could be induced on glass substrates patterned with poly (lysine) micropatterns [34]. Here we demonstrate how substrates with spatially confinement regions of different surface properties ("adhesiveness") can trigger, guide or hinder somal translocation on a biomaterial surface. Using microcontact printed patterns of different adhesive molecules, we control and reproduce neuronal migration phenotypes and terminal ST. The contrasting adherent regions on the substrate can guide and direct ST, and represent a simple yet flexible method to control it by tuning surface interactions. We demonstrate that GC expansion and spreading area are intimately related to the onset of ST. In addition, the process of nucleokinesis towards the GC requires both actin fibers and microtubules to succeed. This novel platform emerges as a promising tool to study the fundamentals of neuronal migration during development and neuronal disorders with dramatic consequences in cortex development, such as lissencephaly with cerebellar hypoplasia (LCH) [3,35].

1. Results

1.1. Terminal somal translocation in vitro triggered by adhesive contrast

We patterned cell adhesive areas onto non-adhesive poly (ethylene glycol) coatings using the micro-contact printing (μCP) method. We selected Poly (lysine) (PL) and Laminin (LN) as adhesive molecules because they are typically used for neuronal cell cultures [30,32,36,37]. These two molecules have very different physicochemical properties: PL is positively charged at neutral pH and does not have any specific biological function [37,38]. LN is an extracellular matrix (ECM) protein that specifically interacts with integrins and other cell membrane receptors [39,40]. We used a 19-mer laminin peptidomimetic (CSRARKQAASIKVAVSADR, abbreviated IK) as an alternative to LN to improve the reproducibility of the μCP process. This peptide effectively supports neurite outgrowth in neuronal cell cultures [41]. Early postmitotic cortical neurons were seeded on PEG substrates printed with 10 μm lines of PL or IK. Cells were mainly attached to the printed PL or IK lines and formed patterns reflecting the adhesive contrast of the surface pattern (Fig. S1a). On the PL lines, neurons adopted a spreading morphology (cell body area 207 ± 42 μm^2) with wide (7.8 ± 1.4 μm) and short (14.9 ± 4.6 μm) neurites (Fig. 1a–d). On the IK patterns cells showed less spreading (148 ± 42 μm^2) and extended thin (1.9 ± 1.1 μm) and long (25.9 ± 18.7 μm) neurites (Fig. 1b-d). Cells remained static on the PL lines, but became bipolar and migrated along the IK lines (Fig. S1b-c). These results suggest a lower exploratory and migratory activity of the cells on the PL patterns,

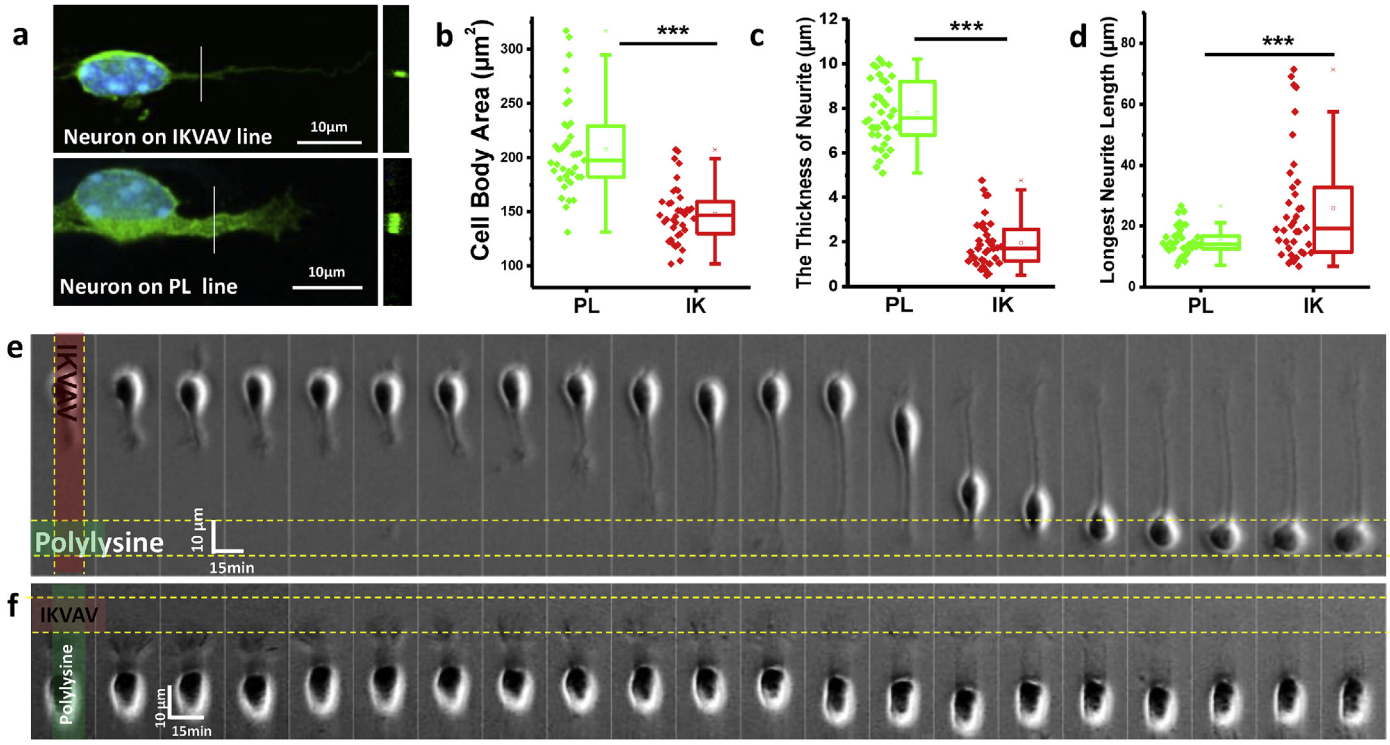

Fig. 1. Somal translocation of embryonic cortical early post-mitotic neurons on PL and IK patterns. (a) Representative image of neurons morphology on PL or IK micro-lines (blue = DAPI, green = SMI, neurofilament marker). Perpendicular scan of the neurite (white line) was performed and images of the YZ optical section are shown for better illustration of neurite thickness (right). (b-d) Quantification of the cell body spreading area (b), the thickness of neurites (c) and the length of longest neurite (d) on PL or IK lines. (e) Time-lapse Images of a neuron on IK line undergoing somal translocation when the leading process finds the PL intersecting line. Pictures (from left to right) were taken every 15 min. (f) Time-lapse Images of a neuron on PL line. The cell remains static, even when the growth cone touches the IK line. Pictures (from left to right) were taken every 15 min. See supplementary video 1 for (e) and (f).(For interpretation of the references to colour in this figure legend, the reader is referred to the web version of this article.)

indicating a stronger attachment.

Supplementary video related to this article can be found at https://doi.org/10.1016/j.biomaterials.2017.11.042.

When PL and IK were combined in crossed line patterns (PL/IK), single neurons on the IK lines underwent somal translocation events. This occurred when the leading process of a neuron growing along the IK line touched a transversal PL line (Fig. 1e and Supplementary Video 1). The GC spread on the intersecting PL line and somal translocation occurred towards the PL region. As the soma moved forward, the leading process remained anchored to the PL area, while a trailing process appeared and eventually developed into a trailing axon (indicated by neurofilament marker in Fig. S2a). After ST, the cell body remained static on the PL line (Fig. S2b). This effect was highly reproducible and was not observed for cells attached to the PL lines (Fig. 1f). These features resemble those observed during somal translocation *in vivo* [4,5,8,9,20]. Our results demonstrate that the PL/IK cross pattern is an *in vitro* scenario that replicates the characteristic features of terminal somal translocation observed *in vivo*.

In order to study the influence of the line geometry in terminal ST, neurons were seeded onto substrates homogeneously coated with IK (background) and with 10 μm PL printed lines. Again, single cells on the IK background underwent ST when the leading process touched a PL line (Fig. 2, Supplementary Videos 2 and 3). Three different phases could be distinguished during ST: During the first phase ($\mathbf{P_1}$) neurons adhering to the IK became multipolar, extending and retracting their neurites and exploring the surrounding area. Eventually, the GC of one of these neurites made contact with a PL μ-line triggering the second phase ($\mathbf{P_2}$) with two main morphological features. First, the process in contact with the PL line becomes the leading process and the cell morphology changes from multipolar to unipolar or bipolar (Supplementary Video 3). Second, the GC of the leading process spreads on the PL μ-line while the leading process becomes straight and thicker. Finally ($\mathbf{P_3}$) the soma was displaced towards the PL line. During and after somal translocation, a remnant of the cell body was left behind and often became the trailing axon (SI Fig. 2a). Notably, the sequence of the morphological alterations was comparable those reported for *in vivo* terminal translocation of early-born pyramidal neurons and other neuronal cell types [8]. These results demonstrate that polarization and somal translocation occurred independently of geometrical guidance (IK microlines), and was only triggered by the adhesiveness contrast between the IK and the PL.

Supplementary video related to this article can be found at https://doi.org/10.1016/j.biomaterials.2017.11.042.

We next asked if the observed behavior was specific for the PL/IK pattern, or if it could be also stimulated by other adhesive molecules. Similar experiments were performed on substrates coated with Collagen IV (COL), Fibronectin (FN) or laminin proteins as background and printed with PL lines (Fig. 3a and S3a). Cells on

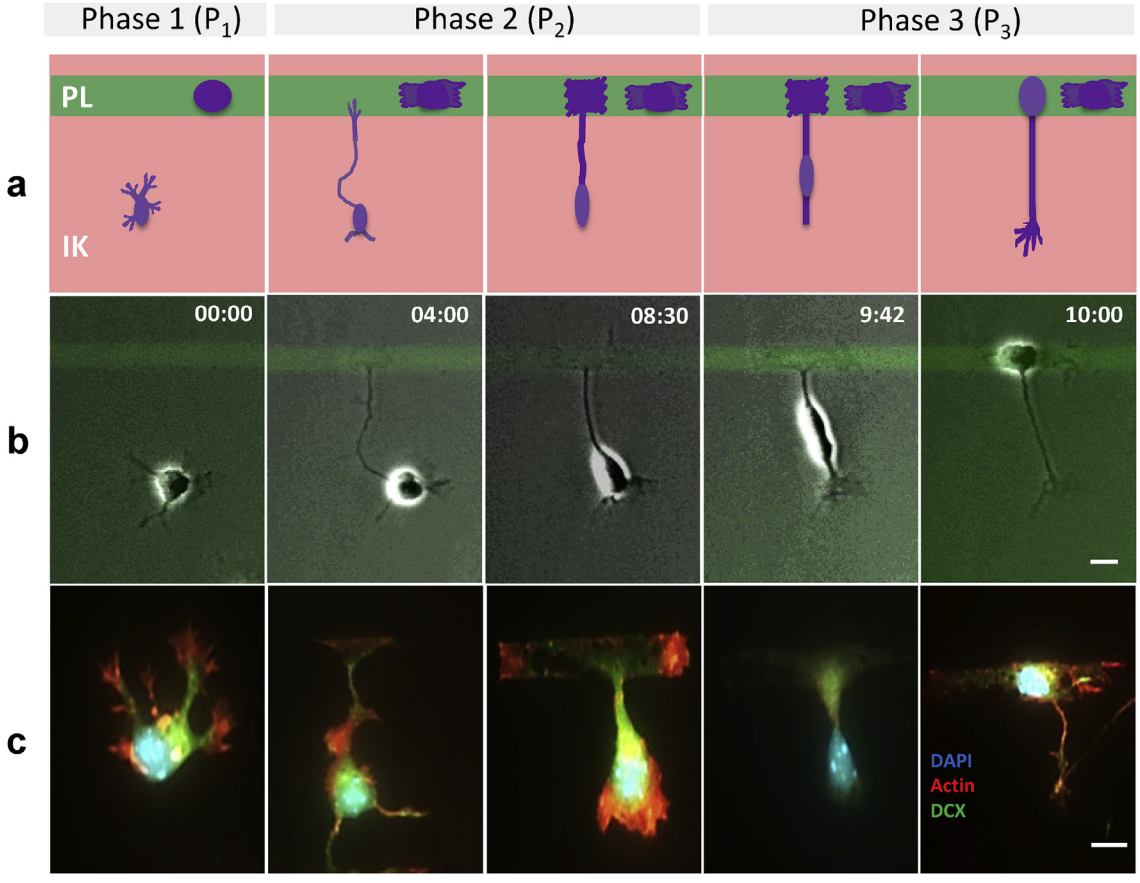

Fig. 2. Phases of neural somal translocation. (a) Schematic showing the 3 phases: P1- cell attached to IK background outgrow neurites until one the tip of one process reaches the PL line by chance. At that point, the neuron polarizes and this process becomes the leading process. P2- The growth cone of the leading process spreads over the PL line. In parallel, remnant neurites are reabsorbed while the leader process becomes more straight and thicker. P3- Cell body moved towards the PL line, leaving a trailing process behinds. **(b)** Time-lapse images of a cell at the three phases. The different time points are indicated as h:min. Fluorescently labeled PL was used for micropatterning. **(c)** Fluorescent images showing F-actin (red) distribution during the different phases of ST. (blue = DAPI, green = neuronal marker, DCX). Scale bar = 10 μm. See also supplementary videos 2 and 3.(For interpretation of the references to colour in this figure legend, the reader is referred to the web version of this article.)

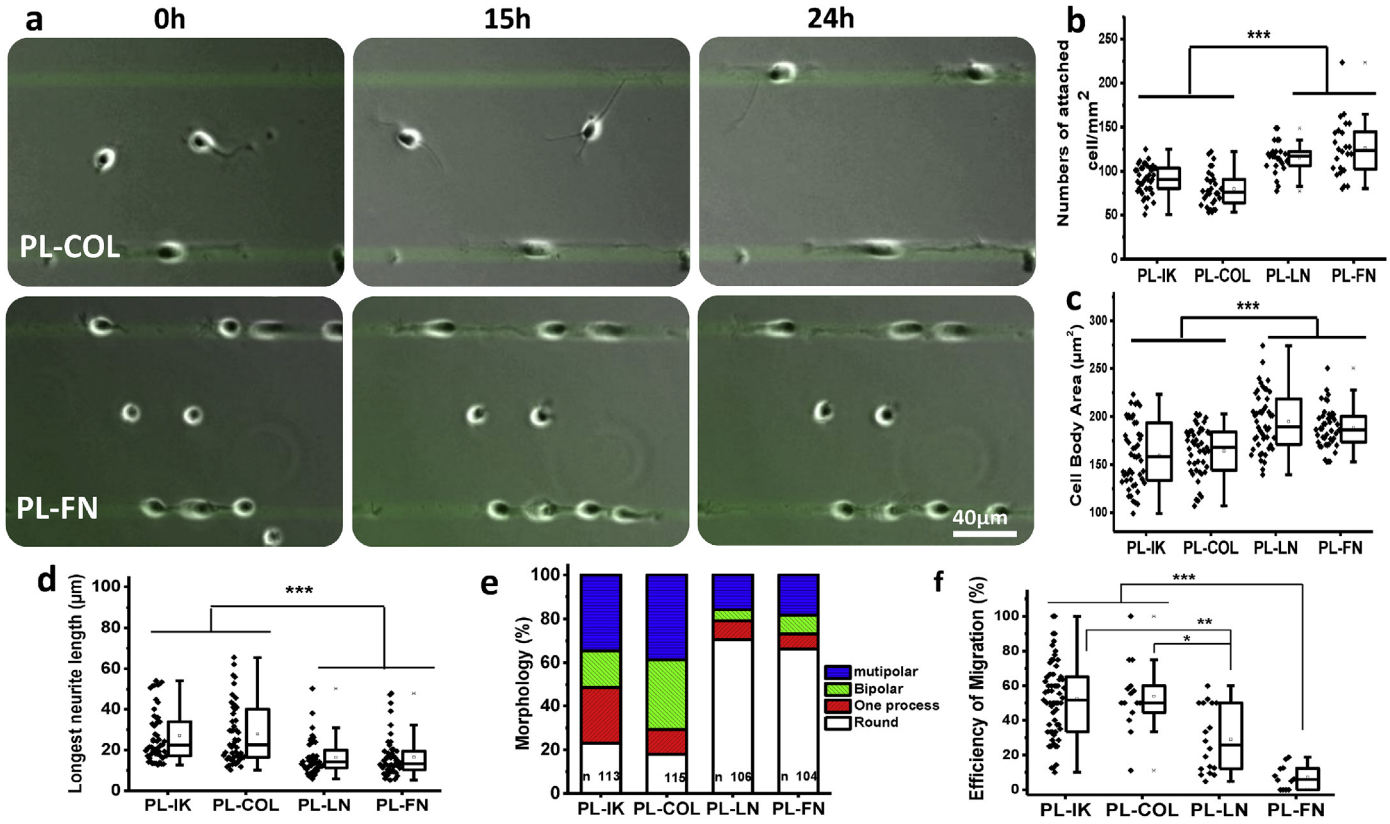

Fig. 3. Influence of different background proteins in neural somal translocation. (a) Time-lapse images showing the cells at 0 and 24 h of time-lapse on PL/Collagen IV (PL/COL) and PL/Fibronectin (PL/FN) coated substrates. Scale bar is 40 μm. Fluorescently labeled PL was used for micropatterning. See Fig. S3 for other adhesive combinations. **(b–f)** Quantification of morphological parameters on the different adhesive combinations: **(b)** Number of attached cell per mm^2 after cell attachment, **(c)** Area of cell body, **(d)** Length of the longest neurite (***$p < 0.001$), **(e)** Percentage of cells attached on background proteins that show rounded, one process, bipolar, or multipolar morphology after 12 h (See also Fig. S4). N = number of quantified cells, and **(f)** ST efficiency (***$p < 0.001$, **$p < 0.01$; *$p < 0.05$). n = quantified areas (708 × 531 $μm^2$).

FN and LN coatings showed larger spreading (Fig. 3c), shorter neurites (Fig. 3d) and preferentially rounded shape (>60%, Fig. 3e). IK and COL coatings favored the development of longer neurites (Fig. 3d, e and S4). Although ST was observed on all adhesive combinations, the frequency of ST events was significantly higher in cells on IK and COL (52.3% and 53.9%) backgrounds compared to LN (28.9%) or FN (7.2%) (Fig. 3f, S3). Cells with multipolar and long neurites explored their surrounding more effectively, increasing the probability or reaching the PL μ-lines. For all patterns, GCs were found to spread on the PL lines to cover similar areas (Fig. S3 b and c). The time that GCs needed for spreading upon reaching the PL line (T_2) and the speed of somal translocation were similar for all adhesive combinations (Fig. S3 d and e). These results demonstrate that the triggering of ST by adhesive contrast is not specific for PL/IK pattern.

We also tested if other adhesive substrates than PL could trigger ST. We printed fibronectin (FN), fibronectin peptidomimetic cyclic (RGDfK) [26,42,43], and Reelin protein [20] lines on IK background. Around 95% of the GCs on PL lines showed large spreading areas, whereas less than 51% of GCs spread on FN, RGD or Reelin lines (Fig. 4a and b). Instead, GCs often showed a branched structure (Fig. 4a). Somal translocation was observed on all patterns, although the efficiency of somal translocation was significantly higher on PL (52.3%) than on RGD (36.5%), Reelin (29.2%) or FN (24.1%) patterns (Fig. 4c and S5). In order to demonstrate a possible correlation between GC spreading and ST efficiency, we quantified the percentage of cells that underwent ST from spreading or branched GC morphologies. ST efficiency was >90% when a spreading GC was formed, while it dropped to 40–55% when the GC showed a branched morphology (Fig. 4d). These results highlight a strong GC-substrate interaction in triggering ST in neurons. The GC spreading time (T_2), and the somal translocation speed (V_3) showed no significant differences among the different protein combinations tested (Fig. S6), indicating that, once activated, the process of somal translocation on the substrates was independent of the type of molecule providing anchoring to the GC and other cell areas.

It should be noted that the concentration of the protein printed on the surface and the PL in our patterns might be different for the different individual combinations. This could also be a reason for the differences in the efficiency of ST among the different proteins, not necessarily the adhesive molecule itself. We asked if adhesive changes caused by the different surface density of the same adhesive molecule could also trigger somal translocation. To address this, we coated background surfaces with different concentrations of PL, and printed microlines with the same concentration of PL as well. Contrast profiles and fluorescent images of printed PL line pattern with background coated with different PL concentration were used to proof the contrast of PL density on the same surface (Fig. S7). After 24 h most cells on surfaces with $1{:}10^{-4}$ and $1{:}10^{-3}$ ($PL_{lines}{:}PL_{background}$, see experimental section for details) patterns underwent ST towards the higher concentrated lines, but little ST was observed on substrates with reduced concentration contrasts (Fig. 5a and b). Neurons were static on surfaces with PL background concentrations $>10^{-2}$ mg/ml (Fig. 5a). Surfaces with lower PL background concentrations $<10^{-3}$ mg/mL favored exploratory phenotypes (Fig. S8) and supported ST efficiently (Fig. 5c). These

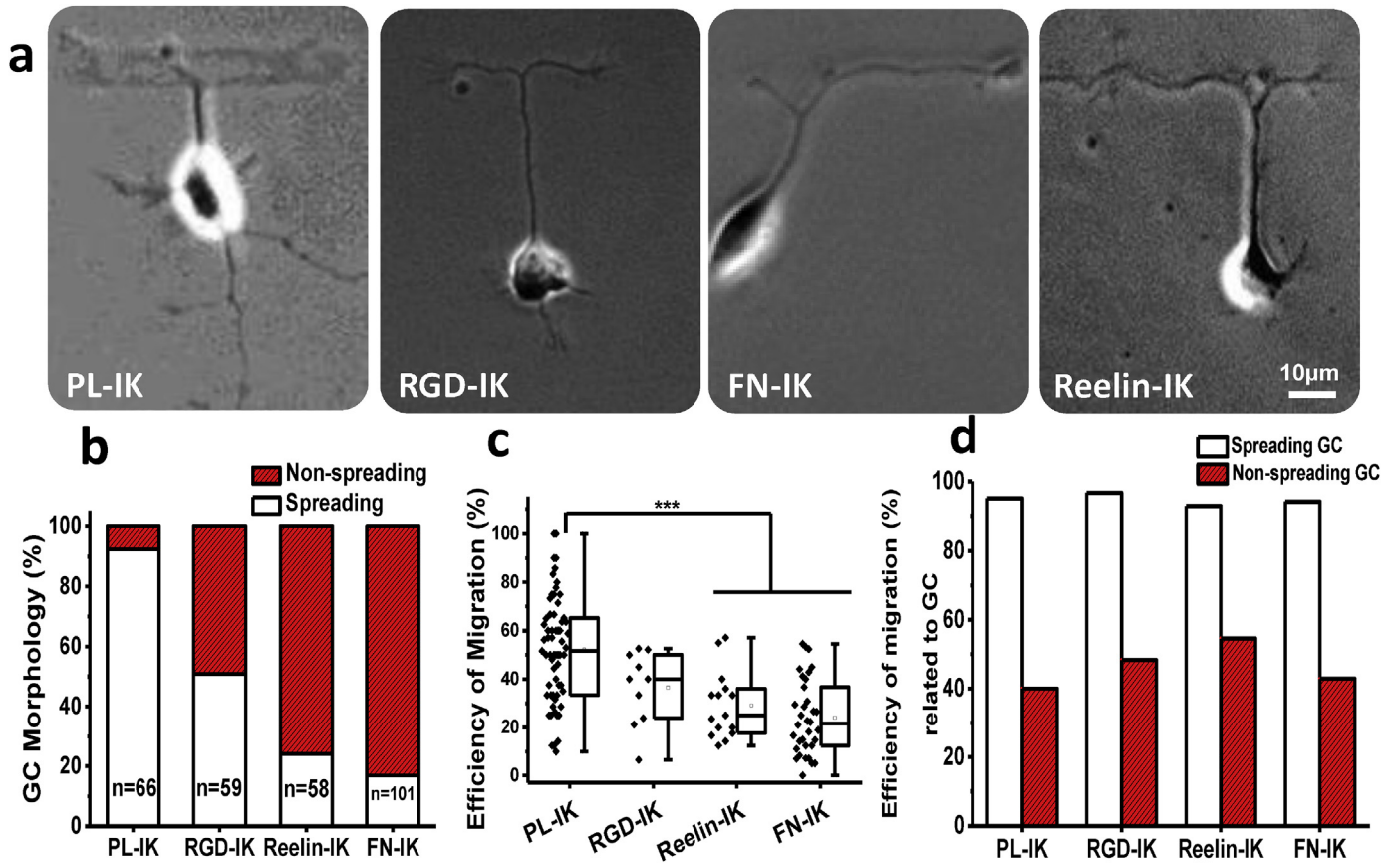

Fig. 4. Influence of different adhesive proteins for triggering neural somal translocation. (a) Microscopy images of the morphology (spread or branched) of the growth cone on PL, FN, RGD or Reelin lines on IK background. Scale bar is 10 μm. (b) The abundance of spread or branched morphologies of the GC on the lines with different adhesive molecules. (c) Efficiency of ST on the different adhesive combinations (***$p < 0.001$). (d) The efficiency of ST for spread or branched GC morphologies (n = 61, 5, 30, 29, 14, 44, 17 and 84).

results confirm that ST can be triggered from surfaces where cells remain exploratory and motile to more adhesive areas where GC spreading occurs. Note that in a previous report Hippocampal neurons seeded on glass substrates were found to migrate to PL patterned areas as well [34]. These findings evince that the adhesive properties of the molecular environment may serve as a key determinant of neuronal ST and neuronal organization during corticogenesis, challenging the view of specific membrane receptor-ligand molecular interactions as triggers for ST. However, with the current data, the role of specific membrane receptor-ligand cannot be completely excluded. Additional work is required to fully discharge specific interactions.

1.2. Spreading of the growth cone determines somal translocation

Supplementary video related to this article can be found at https://doi.org/10.1016/j.biomaterials.2017.11.042.

The central role of the GC during locomotion has been evinced in several reports [30,31]. In our study, the GC spreading on the PL lines to cover areas of 363 ± 117 μm^2, i.e. approximately 5.5 times larger than the area of the GC on the IK coatings (Fig. S9). During the spreading of the GC, the leading process stretched to form a straight line between the anchored GC and the soma, independently of the trajectory of the GC during exploration phase (Fig. 6a, Supplementary Video 4). The stretching process also became wider before ST. These features support a scenario where anchoring and stabilization of the GC on the PL line enable force generation at the leading process for effective translocation of the soma [17,30,31]. We examined if a minimum spreading area is required to mechanically stabilize the GC in order to support ST. IK-coated substrates were printed with PL circles with diameters between 10 μm (78.5 μm^2 area, i.e. the typical size of the GC on IK background) and 20 μm (314 μm^2 area, i.e. the typical size of GC spread on the PL lines) (Fig. 6b, S9, Table S1). When a GC reached PL circles, it spread over the whole adhesive area (Fig. 6c and S10). On 10 μm PL circles approximately 40% of the cells retained multipolar morphologies and 56% failed to translocate their soma after GC spreading. On 20 μm circles, more than 90% of cells developed a single process or a bipolar morphology and underwent ST (Fig. 6d and e and Supplementary Video 5). Intermediate behavior was observed using 15 μm PL circles. These results indicate that the spreading area of the GC strongly affects the efficiency of ST.

Supplementary video related to this article can be found at https://doi.org/10.1016/j.biomaterials.2017.11.042.

1.3. Actin filaments and microtubules are required for somal translocation

Actin and microtubule scaffolds play a major role in the movement of the soma in granular cells [31]. We scrutinized the involvement of actin fibers, myosin contractility, and microtubular structures in ST on our platform by applying different pharmacological treatments: Blebbistatin (Blebb), Latrunculin B (LB), Cytochalasin D (Cyto-D), Y27632 (Y27) or Paclitaxel (PTX) (Fig. S11). We observed drug-treated cells showed higher percentages of round morphologies (21.4% Blebb, 53.8% LB, 36.9% Cyto-D, 62.5% Y27 and

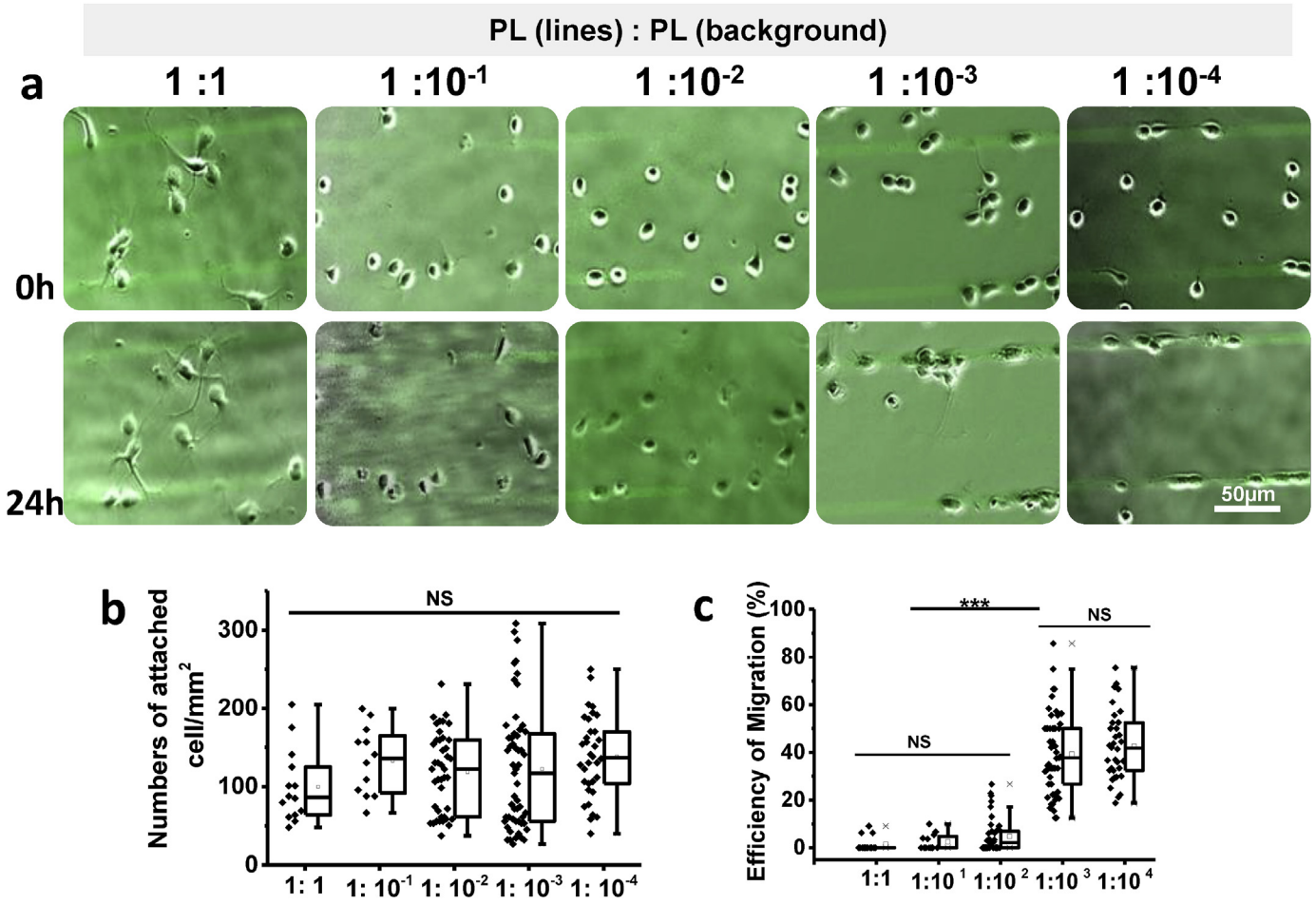

Fig. 5. Adhesive contrast triggers somal translocation. **(a)** The distribution of cells on PL/PL patterns with PL micro-contact printed lines and decreasing PL background concentrations (1:1, $1:10^{-1}$, $1:10^{-2}$, $1:10^{-3}$ and $1:10^{-4}$) at 0 h and 24 h of time-lapse. Scale bar = 50 μm. Fluorescently labeled PL was used for microcontact printing. **(b)** The number of cells attached per mm^2 after cell attachment. **(c)** The efficiency of somal translocation on the different PL/PL patterns (***$p < 0.001$, NS = not significance). n = number of quantified area (708 × 531 μm^2).

33.3%Paclitaxel). The cell body of drug-treated cells occupied larger areas compared to control conditions (Fig. S11a). LB- and Y27-treated neurons displayed significantly shorter neurites than the controls (Fig. S11b). There was a general reduction in GC spreading among the drug-treated cultures (44.4% Blebb, 31.6% LB, 57.9% Cyto-D and 53.1%Paclitaxel) *vs.* the controls (94.7%), with the exception of Y27 (95.8%) (Fig. S11d). In line with this, the efficiency of ST was markedly reduced (1.5–3.8 fold) after most of the drug treatments (Fig. S11e). Our results are in agreement with previous findings showing that both cytoskeletal structures, i.e., actin filaments and microtubules, are needed to mobilize the cell soma [30,31].

2. Discussion

Micropatterned substrates with adjacent areas of different adhesiveness replicate relevant signals found in the natural microenvironment of the developing cerebral cortex and can support, trigger, and spatially guide neuronal somal translocation. The combination of a low-adhesive background and high-adhesive patches stimulated the expansion of long neurites in the former and reproducibly promoted GC expansion and ST to the latter in early postmitotic cortical neurons. This novel platform allowed us to successfully reproduce and quantify the morphological features of ST, including neurite formation and reabsorption, growth cone spreading, thickening of the leading process, and translocation dynamics. This is an ideal *in vitro* model to interrogate environmental cues stimulating neuronal migration with the possibility to study cytoskeletal regulation and organization.

We have found a relationship between substrate properties and morphological parameters to describe neuronal behavior on ST-supporting substrates. On low-adhesive coatings, neurons showed low spreading of the cell body, dynamic neurite growth and retraction, and thin processes. On high-adhesive coatings, neurons displayed a spreading soma and thicker and wider neuronal processes. When the GC of a neuron on a low-adhesive substrate crossed to a high-adhesive area, it spread and ST was triggered. Our adhesive contrast hypothesis is supported by in *vivo* data. Stabilization of the GC of the leading process in the marginal zone is necessary for neuronal migration *in vivo*, and the different concentrations of FN at these zones could be a relevant triggering signal [15,23]. The *in vitro* scenario we propose here is chemically simpler, but it agrees with reported migration behavior of cortical neurons when the leading process anchors near the pia during the radial expansion of the developing cortex [1,9,44,45]. Interestingly, Jiang et al. recently demonstrated that the GC of leading process is attached more strongly than the trailing process during ST [31] consistent with distinct degrees of adhesiveness provided *in vivo*.

Adhesion strength strongly modulates cell migration by providing anchorage and allowing force application and transmission [46]. Polarization and migration directionality are relevant

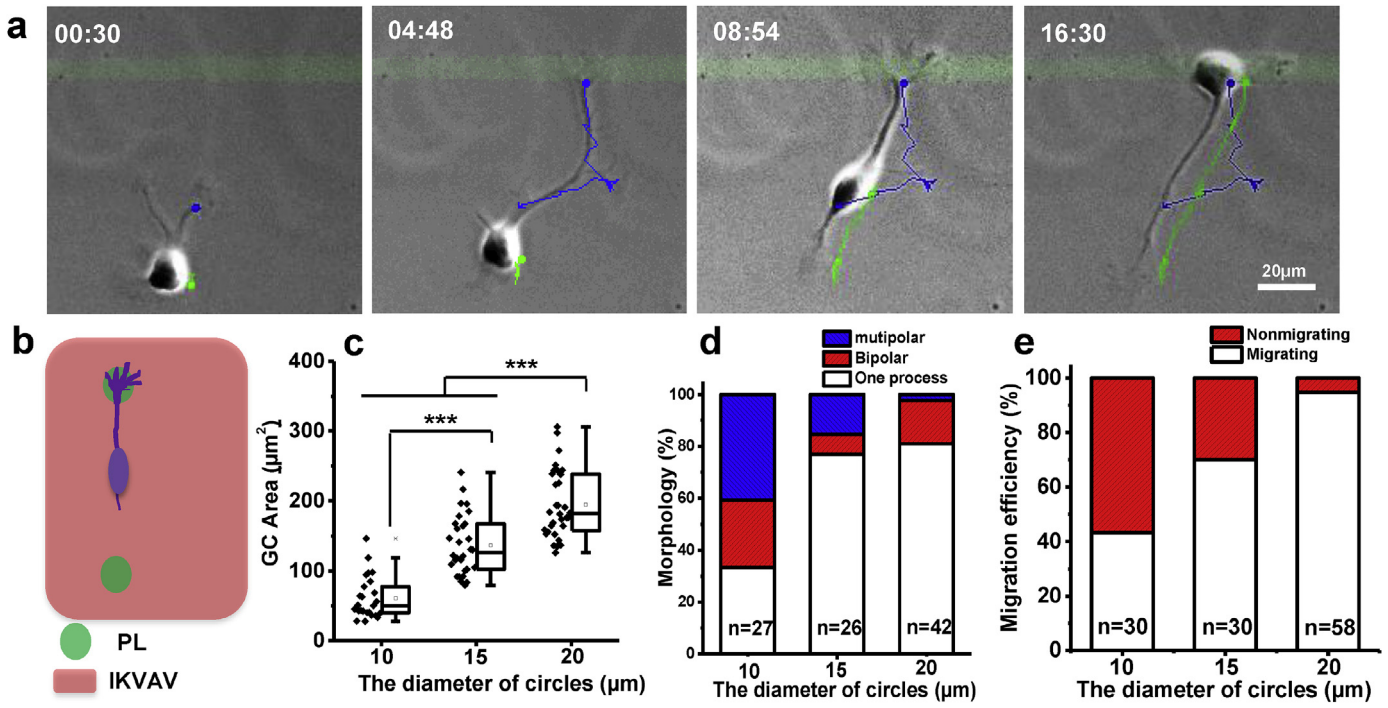

Fig. 6. Spreading of the Growth cone on leading process is a crucial step for somal translocation. (a) Snapshot images (Supplementary Video 4) of a trajectory of a neuron on IK background migrating towards PL line (green fluorescent). Blue and green lines depict the trajectory of the GC and soma respectively. Scale bar corresponds to 20 μm, the different time points are indicated as h:min. (b) Schematic of the PL circle patterns with increasing diameter. (c) Area of the GC on the PL circles of different diameter. (d) The percentage of cells that show one process, bipolar, or multipolar morphology after attachment of their neurites to the PL circles. (e) The efficiency of the somal translocation on the circle patterns of different diameter.(For interpretation of the references to colour in this figure legend, the reader is referred to the web version of this article.)

and are interconnected factors in neuronal migration, and are highly dependent on the adhesive properties of the environment [47]. In neurons, ligand density seems to affect GC directionality [41]. This is particularly relevant in terminal ST, as it could define the final position of the migrating neuron [1,8,9]. Consistent with this data, we demonstrate that the expansion of the GC is associated with the thickening of the leading process as fundamental morphological changes to trigger migratory action. Here we provide a simple experimental microenvironment to study ST under conditions of controlled variable adhesive ligand types and densities, while simultaneously imaging of the cytoskeletal components during the different phases of ST.

We observed the retraction of minor neurites in multipolar cells in correlation with the spreading and anchoring of the leading GC during ST *in vitro*. Remarkably, neurons that found GC expansion limitations also failed to induce the absorption of the other processes. The permanence of these neurites could become a mechanical obstacle that would thwart the formation of an actin contractile rim at the rear of the soma. It has been shown that the actin contractile center forms after the GC expansion and the actin rim were found to be essential to develop ST forces [31]. In light of the sequence of phases during ST observed in our *in vitro* model, we hypothesize that GC expansion not only enhances anchoring but ultimately is the up-stream initiator of the remodeling of the cytoskeleton to support the mechanical tension required for dragging the soma.

3. Conclusion

Elucidating the mechanical requirements and parameters of the molecular environment that regulate migration is crucial for the understanding of the neuronal positioning occurring in the developing brain. We engineered a platform which allows for *in vitro* triggering and studying terminal ST. We demonstrate that ST can be triggered by differential adhesiveness to the substrate. By controlling surface properties, our platform reproduces the morphological features of ST. Our platform will be applied to untangle the molecular mechanisms underlying ST and shed light on the mechanisms of cortical layering and their congenital abnormalities.

4. Methods

4.1. Reagents and materials

N-hydroxysuccinimide (NHS) functionalized Nexterion coverslip H (Schott, Material code: 1098523), silicon gasket (ibidi GmbH, Material code: 81201), Poly-D-lysine (SERVA Electrophoresis GmbH), RGD (cyclo (Arg-Gly-Asp-D-Phe-Lys), peptides international), Recombinant Mouse Reelin (R&D systems), Fibronectin–FITC Labeled (Cytoskeleton, Inc.), 19mer IKVAV (Alfa Aesar), Y27632 (Miltenyi Biotec GmbH) and Cytochalasin D (Santa Cruz Biotechnology) were purchased from specified companies. Poly-L-lysine–FITC Labeled, Laminin, Collagen IV, Blebbistatin, Latrunculin B, and Paclitaxel were purchased from Sigma-Aldrich. All other reagents were obtained from Sigma-Aldrich unless otherwise specified.

4.2. PDMS stamps for microcontact printing

The PDMS stamp for printing was fabricated by standard soft lithography techniques [48]. A SU-8 lithographic template was used for double soft molding to obtain PDMS stamps [49,50]. The SU-8 template was previously functionalized with (1H,1H,2H,2H-perfluorodecyltrichlorosilane) to avoid mold sticking. PDMS precursor (Dow Corning, Sylgard 184) was mixed with 10:1 ratio of prepolymer:curing agent and degassed for 30 min before poured on

the SU-8 template and cured at 90 °C for 1 h. PDMS precursor was poured onto the PDMS soft template and baked at 90 C for 1 h to get the PDMS stamp. Stamps were cut to fit into the wells of the silicon gasket for printing.

4.3. Functionalization of substrates by multistep microcontact printing

Microcontact printing (μCP) technique was used to pattern different proteins onto a Nexterion coverslip H. See Fig. S11 for a detailed description of the method. PDMS stamps were washed with acetone and water by sonication to remove the uncross-linked oligomers and clean the surface. The stamps were treated with oxygen plasma (100 W, 0.1 mbar) for 30s to become more hydrophilic and inked with various peptide or protein solutions (1 mg/ml or 0.1 mg/ml PLL-FITC, 1 mg/ml PDL, 0.1 mg/ml Fibronectin-FITC, 0.1 mg/ml Reelin and 0.1 mg/ml RGD) for 60 min, followed by rinsing with Milli-Q water, and drying with N_2 flow. Only stamps inked with 0.1 mg/mL IK were dried by air drying. The peptide-inked stamps were placed in contact with Nexterion Coverslip H for 60 min, allowing patterned covalent immobilization of the molecules by covalent reaction of their amine groups with the activated carboxylic acids at the Nexterion surface. The Nexterion coverslip was divided into 12 wells (0.56 cm^2 per well) by placing a silicone gasket on the top. After the peeling of the stamp, a second printing step with a different peptide-inked stamp (0.1 mg/mL IKVAV) was performed to obtain a cross pattern. Alternatively, a peptide solution (0.01 mg/ml IKVAV, 0.01 mg/ml Laminin, 0.01 mg/ml collagen IV and 0.01 mg/ml Fibronectin) was incubated Nexterion for 60 min to form line-background pattern. Printing and coupling steps occurred at room temperature and at a relative humidity >80%. Substrates were blocked by immersing in 50 mM ethanolamine in PBS for 60 min, rinsed with water 3 times. Before the cell experiment, the substrates were sterilized by incubated in 70% ethanol for 5 min and rinsed with sterile PBS 3 times.

4.4. Cell isolation and cell seeding

Cerebral cortex from E14.5 of C57BL/6 mice (Janvier-Labs) was digested in 0.5% trypsin EDTA (GIBCO) for 15 min at 37 C. Then trypsin was inactivated by the plating medium (DMEM, GIBCO) and 10% FBS (Hyclone) and gently triturated with a 5-ml disposable pipette to get single cells. After centrifugation at 1000 rpm for 5 min cell pellets were resuspended in 1 ml differentiating medium (DMEM-GIBCO and 2% B27-invitrogen) and seeded directly in the 12 wells at a density of 62 500 cells/ml. The cell density was obtained with a TC20™ Automated Cell Counter (Bio-Rad). After the cells attached, the substrates were imaged by time-lapse microscopy for 24 or 48 h. All animal procedures were carried out in accordance with the Policies on the Use of Animals approved by the Institute of Physiological Chemistry, University Medical Center, Johannes Gutenberg University Mainz.

4.5. Time-lapse microscopy

Video microscopy of neurons was performed with a Cell Observer microscope (Zeiss) at 37 °C and 5% CO_2. Phase contrast images were acquired every 6 min during 2 days using a 20x phase contrast objective (Zeiss) and an AxioCamHRm camera with self-written VBA module remote controlling Zeiss AxioVision 4.7 software. Single-cell tracking and movies assembling were performed using ImageJ 1.42q (National Institute of Health, MD, USA) software.

4.6. Immunostaining and image acquisition

Cells were fixed with 4% paraformaldehyde for 10 min. After washing with PBS three times, cells were pre-incubated with blocking solution (3% BSA and 0.2% Triton X-100 in PBS) at RT for 1 h and then incubated with following primary antibodies overnight at 4 °C: Mouse anti-neuronal filaments (SMI-312, abcam, 1:800 diluted), Guinea Pig anti-DCX (Jackson ImmunoResearch Laboratories, Inc, 1:500). The secondary antibodies (1:1000) were A488-conjugated goat anti-Mouse (Invitrogen) and Cy3-conjugated anti- Guinea Pig (Jackson ImmunoResearch Laboratories, Inc.). For F-actin staining, the cells were incubating with TRITC-labeled phalloidin (Sigma, 1:200). At the end, the cells were mounted by mounting medium containing DAPI (dianova, SCR-038448) on glass slides. Image acquisition was carried out with laser-confocal microscopy (SP5, Leica) using a 63x oil-immersion objective. The z-series were obtained and then visualized as single optical scans with concurrent orthogonal view.

4.7. Drug treatment

Drugs were applied after cells attached on PL/IK patterns and cell behavior was followed for 24 h. The following concentrations were used: 0.1% DMSO (control), Y27632 (Y27; 50 μM), Blebbistatin (Blebb; 50 μM), Latrunculin B (LB; 2 μM), Paclitaxel (PTX; 1 μM) and Cytochalasin D (Cyto-D; 100 nM).

4.8. Imaging and data analysis

The acquired fluorescent images and phase contrast time series were processed and analyzed with Fiji (distribution of ImageJ). For the quantification of the thick of neurite, z-stacks at a slice distance of 0.5 μm were acquired of fixed samples stained for neurofilament marker (SMI) or neuron marker (DCX). To assess the thick of neurite, a line scan perpendicular the neurite was performed and the plot profile of fluorescence was measured to get the FWHM value considered as neurite thickness. The YZ optical section of z-stacks was generated by using the orthogonal view of Fiji.

For the analysis the influence of different ECM component on cells, the following parameters were quantified. i) The number of attached cells per mm^2 as a measure of adhesiveness of the coated protein, ii) the morphology of the cells attached on background (rounded, multipolar, bipolar, single process) [51] after 12 h culture, iii) the length of the longest neurite attached on background after 12 h culture as indicators of polarized or exploratory status of the cells, and iv) the percentage of cells undergoing neural somal translocation towards the PL lines during 24 h as an indicator of the efficiency of the ST process. Briefly, a phase contrast time series ($708 \times 531\ \mu m^2$) in a period of 24 h was used to calculate (Fig. S12). The number of cell adhesion is the number of cells which attach to the substrate at the beginning of Time-lapse (0 h). The cell migration efficiency (Efficiency), the cells which migrate to line protein (M) after 24 h, and all the cells which located between lines (background) at the beginning of time-lapse (A) defined as:

$$\text{Efficiency} = M/A$$

The time of Phase 2 (T_2) corresponded to the spreading time of GC. The speed of the ST corresponds to the ratio between the length of leading process at the beginning of somal translocation (d_1), and the time of phase 3 (T_3):

$$\text{Speed} = d1/T3$$

Cell trajectories were recorded with the Fiji MTrackJ plug-in. Every slide of the position of cell body or GC was marked by

manually clicking on the cell. The migration efficiency related to the GC morphology is defined as the percentage of cells (M − S) that display spreading GC and migrate to line pattern divided by all cells that found the line pattern by spreading GC (A-S).

Efficiency = M-S/A-S

Or the percentage of cells (M − B) that form branching GC and migrate to line pattern divided by all cells that found the line pattern by branching GC (A-B).

Efficiency = M-B/A-B

For circle pattern, the migration efficiency (Efficiency-Circ) is defined as the percentage of cells (M-Circ) that migrate to PL circles divided by all cells that found the PL circles by neurites (A-Circ):

Efficiency-Circ = M-Circ/A-Circ

In the PL circle experiment, the morphology of cell was measured by the percentage of cells that showed one process, bipolar, or multipolar morphology after the neurites attached to PL circles. For migrating cells, the morphology was defined when the soma started to migrate. For a non-migrating cell, the shape of the cell was chosen at the end of time-lapse (24 h).

4.9. Statistical analysis

For each condition, a minimum of three independent experiments was performed. Data were expressed as mean ± standard deviation. Box plots represent the middle 50% of data between the 1st to the 3rd quartile (interquartile range IQR); the whiskers indicate variability outside the upper and lower quartiles. One-way ANOVA was used to determine significance between groups followed by a post-hoc Tukey contrast (GraphPad Software). For non-parametric data, we performed Kruskal-Wallis analysis followed by Dunn's post-hoc multiple comparisons. All the cases a value of $p < 0.05$ was used for statistical significance.

Author contributions

MJS and AdC conceived the project. SZ, WF, MJS, BB and AdC contributed with the experimental design. SZ and WF performed most of the experimental work. XG contributed to data quantification. LX contributed experimentally to the lithography and printing processes. SZ, MJS, BB and AdC contributed to manuscript writing.

Acknowledgements

The authors acknowledge Susanne Selzer for help with soft lithography. China Scholarship Council (201306630012) is acknowledged for its financial support to SZ and WF. Work by MJS was supported by an internal grant (Stufe 1) from the Johannes Gutenberg University Mainz. Work in the BB lab was supported by the Belgian Science Policy Office (IUAP-VII/20 “WiBrain”) and an ERA-NET NEURON grant (01EW1604 “ImprovVision”).

Appendix A. Supplementary data

Supplementary data related to this article can be found at https://doi.org/10.1016/j.biomaterials.2017.11.042.

References

[1] K. Sekine, K.i. Kubo, K. Nakajima, How does Reelin control neuronal migration and layer formation in the developing mammalian neocortex? Neurosci. Res. 86 (2014) 50–58.
[2] R. Ayala, T. Shu, L.-H. Tsai, Trekking across the brain: the journey of neuronal migration, Cell 128 (1) (2007) 29–43.
[3] A. Gupta, L.-H. Tsai, A. Wynshaw-Boris, Life is a journey: a genetic look at neocortical development, Nat. Rev. Genet. 3 (5) (2002) 342–355.
[4] B. Nadarajah, J.G. Parnavelas, Modes of neuronal migration in the developing cerebral cortex, Nat. Rev. Neurosci. 3 (6) (2002) 423–432.
[5] B. Nadarajah, J.E. Brunstrom, J. Grutzendler, R.O. Wong, A.L. Pearlman, Two modes of radial migration in early development of the cerebral cortex, Nat. Neurosci. 4 (2) (2001) 143–150.
[6] P. Rakic, Mode of cell migration to the superficial layers of fetal monkey neocortex, J. Comp. Neurol. 145 (1) (1972) 61–83.
[7] K. Sekine, T. Honda, T. Kawauchi, K.I. Kubo, K. Nakajima, The outermost region of the developing cortical plate is crucial for both the switch of the radial migration mode and the Dab1-dependent “Inside-Out” lamination in the neocortex, J. Neurosci. 31 (25) (2011) 9426–9439.
[8] O. Marín, M. Valiente, X. Ge, L.-H. Tsai, Guiding neuronal cell migrations, Cold Spring Harb. Perspect. Biol. 2 (2) (2010), a001834.
[9] J.A. Cooper, Mechanisms of cell migration in the nervous system, J. Cell Biol. 202 (5) (2013) 725–734.
[10] W. Wu, K. Wong, J.H. Chen, Z.H. Jiang, S. Dupuis, J.Y. Wu, Y. Rao, Directional guidance of neuronal migration in the olfactory system by the protein Slit, Nature 400 (6742) (1999) 331–336.
[11] M.E. Hatten, New directions in neuronal migration, Science 297 (5587) (2002) 1660–1663.
[12] O. Marın, A. Yaron, A. Bagri, M. Tessier-Lavigne, J.L.R. Rubenstein, Sorting of striatal and cortical interneurons regulated by semaphorin-neuropilin interactions, Science 293 (5531) (2001) 872–875.
[13] M. Trommsdorff, M. Gotthardt, T. Hiesberger, J. Shelton, W. Stockinger, J. Nimpf, R.E. Hammer, J.A. Richardson, J. Herz, Reeler/Disabled-like disruption of neuronal migration in knockout mice lacking the VLDL receptor and ApoE receptor 2, Cell 97 (6) (1999) 689–701.
[14] F. Tissir, A.M. Goffinet, Reelin and brain development, Nat. Rev. Neurosci. 4 (6) (2003) 496–505.
[15] K. Sekine, T. Kawauchi, K.I. Kubo, T. Honda, J. Herz, M. Hattori, T. Kinashi, K. Nakajima, Reelin controls neuronal positioning by promoting cell-matrix adhesion via inside-out activation of integrin α5β1, Neuron 76 (2) (2012) 353–369.
[16] G. D'Arcangelo, Reelin in the years: controlling neuronal migration and maturation in the mammalian brain, Adv. Neurosci. 2014 (2014) 19.
[17] X. Chai, L. Fan, H. Shao, X. Lu, W. Zhang, J. Li, J. Wang, S. Chen, M. Frotscher, S. Zhao, Reelin induces branching of neurons and radial glial cells during corticogenesis, Cereb. Cortex 25 (10) (2015) 3640–3653.
[18] X. Chai, E. Förster, S. Zhao, H.H. Bock, M. Frotscher, Reelin stabilizes the actin cytoskeleton of neuronal processes by inducing n-cofilin phosphorylation at serine3, J. Neurosci. 29 (1) (2009) 288–299.
[19] M. Frotscher, Role for Reelin in stabilizing cortical architecture, Trends Neurosci. 33 (9) (2010) 407–414.
[20] J.A. Cooper, A mechanism for inside-out lamination in the neocortex, Trends Neurosci. 31 (3) (2008) 113–119.
[21] K. Ishii, K.-i. Kubo, K. Nakajima, Reelin and neuropsychiatric disorders, Front. Cell. Neurosci. 10 (229) (2016).
[22] Y. Jossin, J.A. Cooper, Reelin, Rap1 and N-cadherin orient the migration of multipolar neurons in the developing neocortex, Nat. Neurosci. 14 (6) (2011) 697–703.
[23] S.J. Franco, I. Martinez-Garay, C. Gil-Sanz, S.R. Harkins-Perry, U. Müller, Reelin regulates cadherin function via Dab1/Rap1 to control neuronal migration and lamination in the neocortex, Neuron 69 (3) (2011) 482–497.
[24] L. Dulabon, E.C. Olson, M.G. Taglienti, S. Eisenhuth, B. McGrath, C.A. Walsh, J.A. Kreidberg, E.S. Anton, Reelin binds α3β1 integrin and inhibits neuronal migration, Neuron 27 (1) (2000) 33–44.
[25] K. Sanada, A. Gupta, L.-H. Tsai, Disabled-1-Regulated adhesion of migrating neurons to radial glial fiber contributes to neuronal positioning during early corticogenesis, Neuron 42 (2) (2004) 197–211.
[26] M.J. Salierno, A.J. García, A. del Campo, Photo-activatable surfaces for cell migration assays, Adv. Funct. Mater. 23 (48) (2013) 5974–5980.
[27] M.J. Salierno, L. García-Fernandez, N. Carabelos, K. Kiefer, A.J. García, A. del Campo, Phototriggered fibril-like environments arbitrate cell escapes and migration from endothelial monolayers, Biomaterials 82 (2016) 113–123.
[28] L.A.B. Elias, D.D. Wang, A.R. Kriegstein, Gap junction adhesion is necessary for radial migration in the neocortex, Nature 448 (7156) (2007) 901–907.
[29] M. Arnold, V.C. Hirschfeld-Warneken, T. Lohmüller, P. Heil, J. Blümmel, E.A. Cavalcanti-Adam, M. López-García, P. Walther, H. Kessler, B. Geiger, J.P. Spatz, Induction of cell polarization and migration by a gradient of nanoscale variations in adhesive ligand spacing, Nano Lett. 8 (7) (2008) 2063–2069.
[30] M. He, Z.H. Zhang, C.B. Guan, D. Xia, X.B. Yuan, Leading tip drives soma translocation via forward F-actin flow during neuronal migration, J. Neurosci. 30 (32) (2010) 10885–10898.

[31] J. Jiang, Z.H. Zhang, X.B. Yuan, M.M. Poo, Spatiotemporal dynamics of traction forces show three contraction centers in migratory neurons, J. Cell Biol. 209 (5) (2015) 759–774.
[32] S. Joo, K. Kang, Y. Nam, In vitro neurite guidance effects induced by polylysine pinstripe micropatterns with polylysine background, J. Biomed. Mater. Res. Part A 103 (8) (2015) 2731–2739.
[33] S. Joo, J.Y. Kim, E. Lee, N. Hong, W. Sun, Y. Nam, Effects of ECM protein micropatterns on the migration and differentiation of adult neural stem cells, Sci. Rep. 5 (2015).
[34] J. Corey, B. Wheeler, G. Brewer, Compliance of hippocampal neurons to patterned substrate networks, J. Neurosci. Res. 30 (2) (1991) 300–307.
[35] S.E. Hong, Y.Y. Shugart, D.T. Huang, S.A. Shahwan, P.E. Grant, J.O. Hourihane, N.D. Martin, C.A. Walsh, Autosomal recessive lissencephaly with cerebellar hypoplasia is associated with human RELN mutations, Nat. Genet. 26 (1) (2000) 93–96.
[36] L.A. Flanagan, L.M. Rebaza, S. Derzic, P.H. Schwartz, E.S. Monuki, Regulation of human neural precursor cells by laminin and integrins, J. Neurosci. Res. 83 (5) (2006) 845–856.
[37] D. Mazia, G. Schatten, W. Sale, Adhesion of cells to surfaces coated with polylysine. Applications to electron microscopy, J. cell Biol. 66 (1) (1975) 198–200.
[38] A. Ruiz, L. Buzanska, D. Gilliland, H. Rauscher, L. Sirghi, T. Sobanski, M. Zychowicz, L. Ceriotti, F. Bretagnol, S. Coecke, Micro-stamped surfaces for the patterned growth of neural stem cells, Biomaterials 29 (36) (2008) 4766–4774.
[39] P.E. Hall, J.D. Lathia, M.A. Caldwell, C. ffrench-Constant, Laminin enhances the growth of human neural stem cells in defined culture media, BMC Neurosci. 9 (1) (2008) 71.
[40] M. Manthorpe, E. Engvall, E. Ruoslahti, F.M. Longo, G.E. Davis, S. Varon, Laminin promotes neuritic regeneration from cultured peripheral and central neurons, J. Cell Biol. 97 (6) (1983) 1882–1890.
[41] D.N. Adams, E.Y.C. Kao, C.L. Hypolite, M.D. Distefano, W.S. Hu, P.C. Letourneau, Growth cones turn and migrate up an immobilized gradient of the laminin IKVAV peptide, J. Neurobiol. 62 (1) (2005) 134–147.
[42] T.T. Lee, J.R. García, J.I. Paez, A. Singh, E.A. Phelps, S. Weis, Z. Shafiq, A. Shekaran, A. del Campo, A.J. García, Light-triggered in vivo activation of adhesive peptides regulates cell adhesion, inflammation and vascularization of biomaterials, Nat. Mater. 14 (3) (2015) 352–360.
[43] R. Pankov, K.M. Yamada, Fibronectin at a glance, J. Cell Sci. 115 (20) (2002) 3861–3863.
[44] C.C. Gertz, A.R. Kriegstein, Neuronal migration dynamics in the developing Ferret cortex, J. Neurosci. 35 (42) (2015) 14307–14315.
[45] V. Fernández, C. Llinares-Benadero, V. Borrell, Cerebral cortex expansion and folding: what have we learned? EMBO J. 35 (10) (2016) 1021–1044.
[46] J.T. Parsons, A.R. Horwitz, M.A. Schwartz, Cell adhesion: integrating cytoskeletal dynamics and cellular tension, Nature reviews, Mol. cell Biol. 11 (9) (2010) 633–643.
[47] J.V. Small, T. Stradal, E. Vignal, K. Rottner, The lamellipodium: where motility begins, Trends Cell Biol. 12 (3) (2002) 112–120.
[48] Y. Xia, G.M. Whitesides, Soft lithography, Angew. Chem. Int. Ed. 37 (5) (1998) 550–575.
[49] A.D. Campo, C. Greiner, SU-8: a photoresist for high-aspect-ratio and 3D submicron lithography, J. Micromech. Microeng. 17 (6) (2007) R81.
[50] C. Greiner, A. del Campo, E. Arzt, Adhesion of bioinspired micropatterned Surfaces: effects of Pillar Radius, aspect ratio, and preload, Langmuir 23 (7) (2007) 3495–3502.
[51] S. Tahirovic, F. Bradke, Neuronal polarity, Cold Spring Harb. Perspect. Biol. 1 (3) (2009), a001644.